Science Advances
AAAS

Supplementary Materials for

AI-aided geometric design of anti-infection catheters

Tingtao Zhou *et al.*

Corresponding author: Paul W. Sternberg, pws@caltech.edu; Chiara Daraio, daraio@caltech.edu

Sci. Adv. **10**, eadj1741 (2024)
DOI: 10.1126/sciadv.adj1741

The PDF file includes:

Other Supplementary Material for this manuscript includes the following:

Supplementary Text

Example bacteria trajectories under different geometric and flow conditions

In Fig. S1 we show a few more example trajectories of Brownian bacteria. Comparing Fig. S1(A) with (C), without flow the asymmetric obstacle shape provides an additional rectification effect. Comparing Fig. S1(A)(C) to (B)(D), the flow vorticity provides a significant additional disruption to redirect the bacteria.

Fluid vortices around the tip of obstacles

In Fig. S2 we show how the relative size and spacing of obstacles affect the effective vorticity of the fluid flow. To make fair comparisons, we measure the maximum vorticity and then normalize it by the effective flow speed

$$\widetilde{\Omega} = \frac{a\Omega}{U_0}$$

where a is the particle diameter. The effective flow speed is measured as the minimum value along the center line of the channel, with the channel width W.

Fig. S2 (A)(B) compare the limits of small and large inter-obstacle distance d. In the limit of very large separation between neighboring obstacles (Fig. S2 B), the vortices are independent of each other and saturate to a constant as d/W increases (Fig. S2 G). However, when the vortices are brought very close to each other (Fig. S2A), they start to interfere and the resulting effective vorticity is reduced as d decreases (Fig. S2 G). Hence there exists a threshold value for the inter-obstacle distance such that the vortices do not overlap and fully develop. This condition is beneficial to the suppression mechanism as stronger vortices can disrupt the upstream swimming trajectories more. Fig. S2 (C-F) show the enhancement of effective vorticity as the obstacle height h increases. This is due to two reasons: (1) The flow lines are 'pinched' when passing over an obstacle, such that the flow speed at the obstacle tip is enhanced, which is proportional to the vorticity. (2) The more acute angle of the tip (a larger effective local curvature) induces a stronger 'bending' of the flow lines. However, the height should not be arbitrarily large: the pressure drop will increase significantly as a larger h indicates a smaller effective channel width, as shown in Fig. S2(F). In the limit of $h = W/2$, the channel is completely blocked by the obstacles and the pressure drop required to flow diverges.

Considering all these effects, together with the fabrication accuracy of microfluidics, we formulated the constraint optimization problem as described in the main text and Materials and Methods.

Geo-FNO aided design optimization

Anti-infection catheter design is essentially a partial differential equation constraint optimization problem. However, solving these design optimization problems requires repeatedly evaluating computational models to explore the design space. Hence, the present coupled fluid particle simulation, which takes about 10 minutes, is expensive or even unaffordable for this purpose. Moreover, design optimization generally requires an adjoint solver to compute the gradient for efficient optimization algorithms, but the randomness introduced by the Levy RTP model makes it impractical to implement. All these challenges motivated us to consider machine learning-based surrogate models, Geo-FNO, to accelerate the design optimization process. We train the Geo-FNO model on 1000 simulations uniformly generated from our design space, and test it on 100 randomly generated designs. The model takes the shape of the channel as the input, and outputs the bacteria density as a 1D function. The training error and test error are depicted in Fig.

S3, no overfitting is observed, and the average relative test error is about 4%. After training, Each evaluation of the map from the channel geometry to the bacterial population takes only 0.005 seconds on GPUs in contrast to 10 minutes by using coupled fluid-particle simulations, and therefore it is affordable to do thousands of evaluations in the optimization procedure.
For the optimization, the forward map takes these four design parameters d, L, h, s, generates channel geometry, predicts the bacteria population with Geo-FNO, and finally computes the objective function $\langle x_{up} \rangle$. Automatic differentiation tools embedded in the deep learning package (i.e., Pytorch) are used to efficiently compute gradients with respect to design variables enabling the use of gradient-based design optimization methods. We start from initial design parameters $(d = 100, h = 25, s = 10, L = 20)$ μm, and update them using the BFGS algorithm with Strong Wolfe line search to minimize the objective function $\langle x_{up} \rangle$. To enforce the constraints about these design parameters, exponential transforms are applied to the design parameters. For example to enforce $x_{min} \leq x \leq x_{max}$, x is defined as $x = \varphi(\theta) = x_{min} + (x_{max} - x_{min})/(1 + e^{\theta})$. This ensures that Geo-FNO remains in the interpolation regime and the final design satisfies manufacturing conditions. Another challenge is related to local minimizers, since most partial differential constraint optimization is non-convex. When the optimization gets trapped in a local minimizer, the optimization restarts from an initial condition obtained by perturbing the recorded-global minimizer with a random Gaussian noise sampled from $N(0, I)$. The optimization loss vs. Optimization iteration curve is depicted in Fig. S3B. The recorded-global minimizer is obtained at about 1500 iterations, the loss is reduced from $\langle x_{up} \rangle = 6.68 \times 10^5$ to $\langle x_{up} \rangle = 2.18 \times 10^5$. Several cross-sections of the loss function landscape around the final optimized design are presented in Fig. S3C-E. The Geo-FNO model is more interpretable as opposed to a black box model that directly outputs design parameters for shapes of the triangles in the catheter, without estimating the full flow field. Further, Geo-FNO is more accurate than the simpler black box model (a standard multi-layer perceptron or MLP) that directly predicts the design parameters. With the same amount of training dataset, Geo-FNO gets a 2.5% error on averaged bacteria density, while MLP gets a 3.1% error.
Within imposed parameter constraints, the landscape near the optimized design is neither convex nor monotonic with respect to these design variables, but the loss is generally smaller with larger h, larger s, smaller d, which indicates the channel design is more effective when the height of the obstacle is large, the tip points towards downstream, and obstacle is more frequent.

Bacteria supercontamination in all flow rates in 3D macroscopic experiments
In Fig. S4 we show the super-contamination measured in all 3 flow rates.

Bacterial colony counting method
In the macroscopic experiments, we counted the number of bacterial colonies on the plates after curing them for 24 hrs at room temperature. Four round areas of equal size (8mm diameter) were selected, as shown in Fig. S5, and only the colonies within these areas are counted. We then multiplied the result by the ratio of the total plate area (8cm diameter) / counting areas = 25 to estimate the total number of colonies. When too many colonies are present on a plate, it becomes impossible to distinguish them and we denoted the number of colonies as an arbitrarily large number 30000.

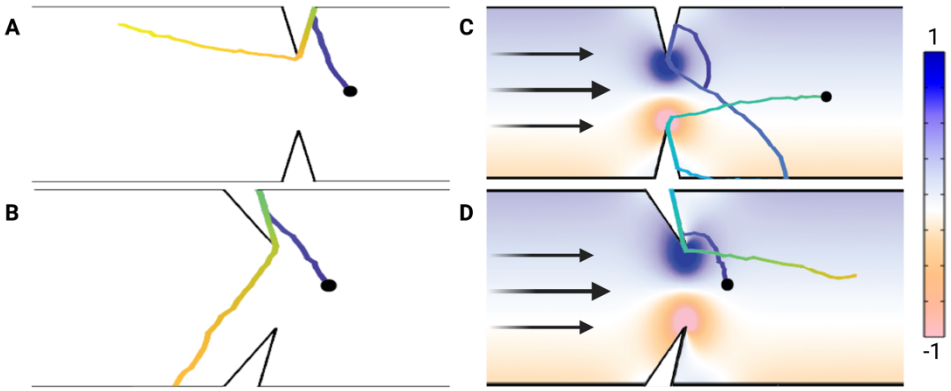

Fig. S1. Example simulated trajectories of active Brownian particles. Trajectories in channels with (A)(C) symmetric obstacles and (B)(D) asymmetric obstacles. (A)(B) without fluid flow. (C)(D) with the fluid flow. Color indicates local normalized vorticity.

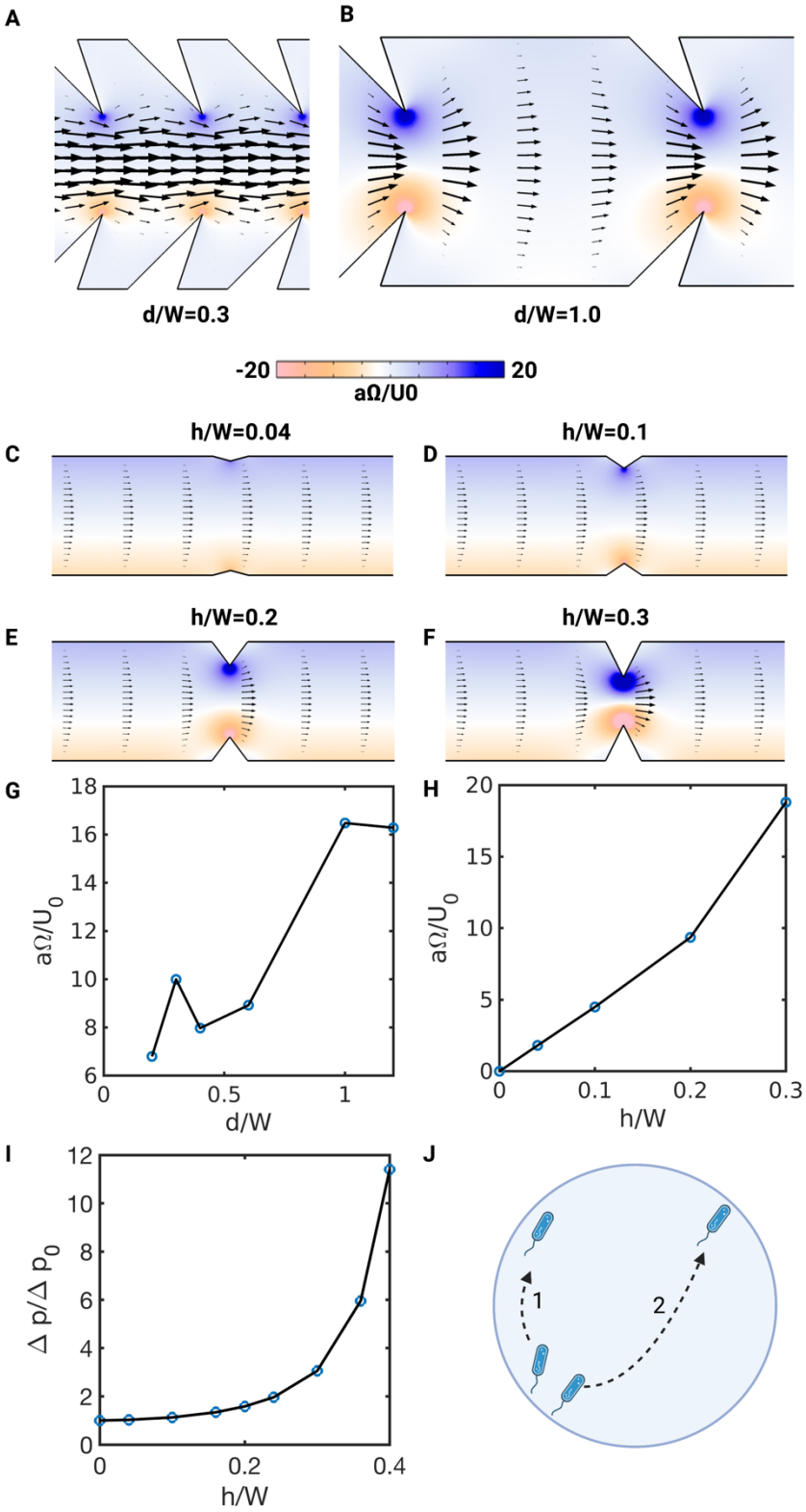

Fig. S2. Considerations for geometric optimization constraints and scaling. (A-H) Normalized vorticity as a function of the obstacle height h and the distance between obstacles d. (I) Normalized pressure drop over one period along the channel as a function of the normalized obstacle height h/W. (J) Cross-section view of bacteria motion inside a macroscopic cylindrical

tube. Compared to trajectory 2, where the bacterium experiences strong down-stream flow near the center of the tube, the other bacterium taking the trajectory 1 stays close to the wall. As a result, bacterium 1 experiences flow conditions more similar to those we considered in the microfluidic channel. The upstream swimming behavior and geometric suppression mechanism will be similar to the microfluidic condition, with only quantitative modifications.

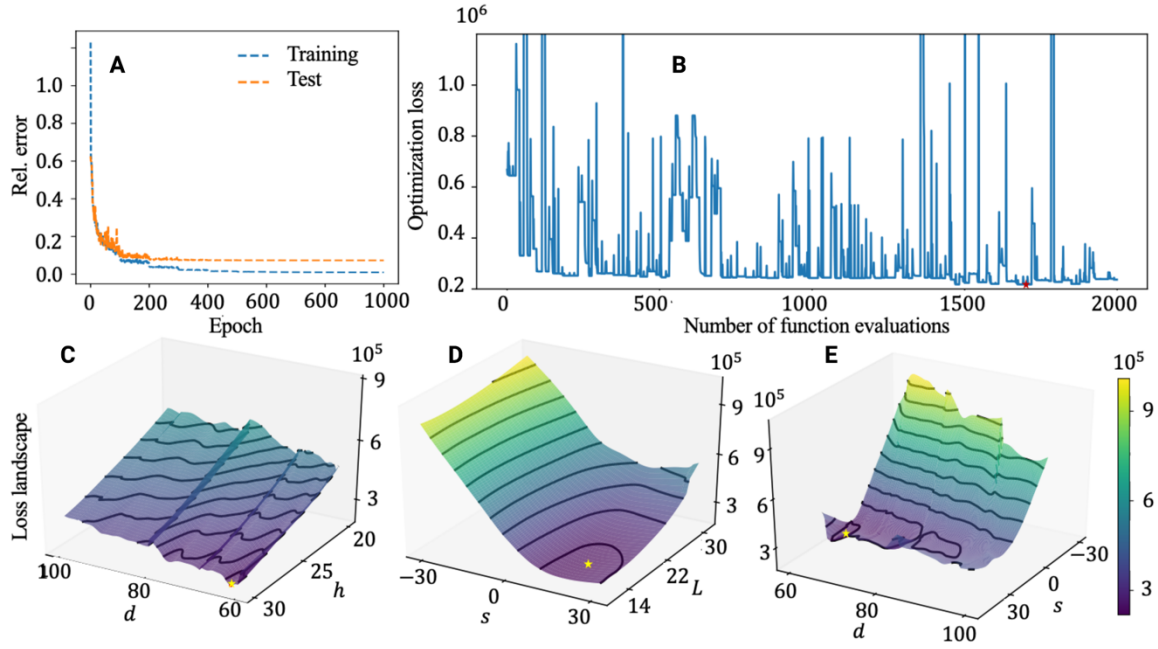

Fig. S3.

Optimization details. A. Training and test errors for Geo-FNO, both errors converge without overfitting; B. Optimization loss obtained by the randomized BFGS algorithm accelerated by our Geo-FNO surrogate model, the recorded-global loss is obtained at about 1500 iterations. C. Visualization of the loss landscape around the optimized design at the $d - h$ cross-section obtained by Geo-FNO; D. Visualization of the loss landscape around the optimized design at the $s - L$ cross section obtained by Geo-FNO; E. Visualization of the loss landscape around the optimized design at the d-s cross-section obtained by Geo-FNO.

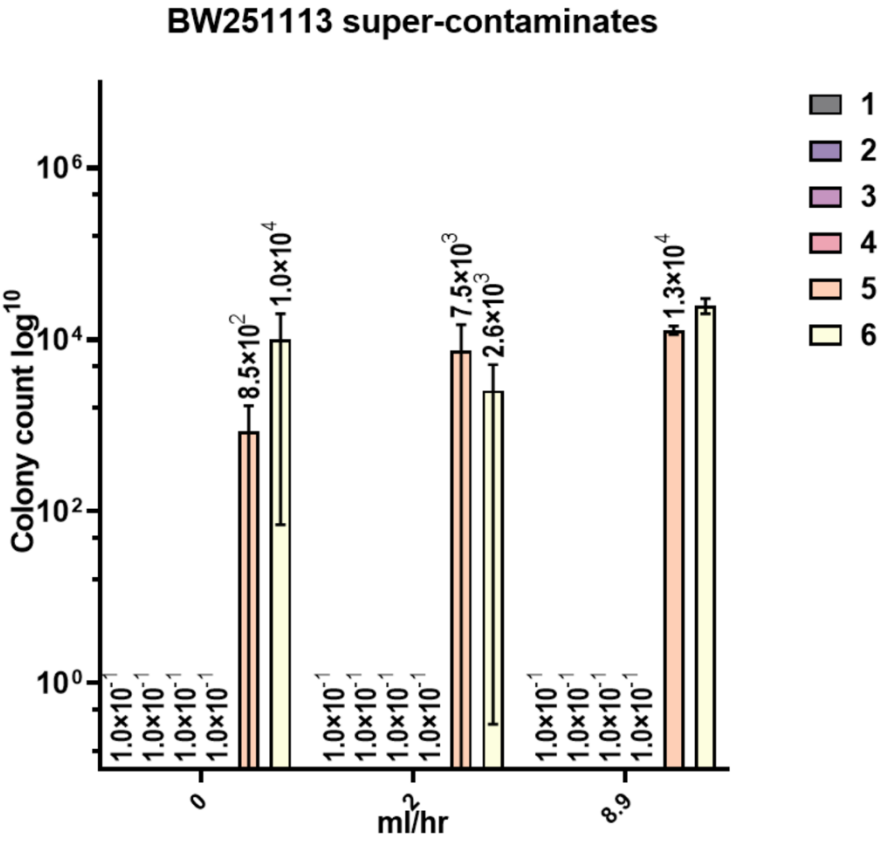

Fig.S4. Super-contamination measured in all 3 flow rates.

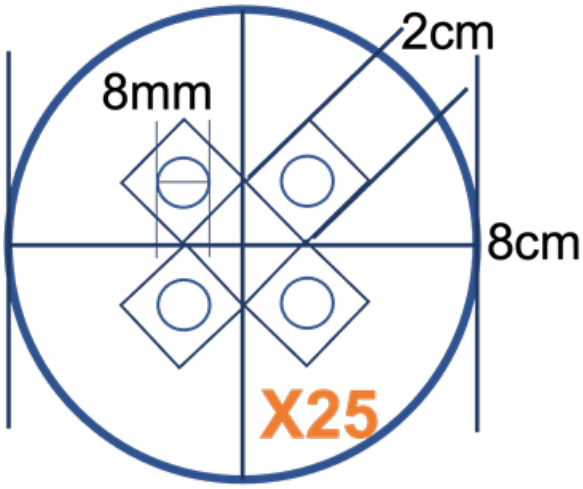

Fig.S5. Schematic of bacterial colony counting method on culturing plates.

Movie S1.-S2. Recording of bacteria detachment from the walls under various flow conditions.

Movie S3. Real-time design optimization.